Please cite the Published Version

Mazzotta, A, Taccola, S , Cesini, I, Sanchez Sifuentes, M, Harris, RA , and Mattoli, V (2025) Low-voltage wearable tactile display with thermo-pneumatic actuation. Npj Flexible Electronics, 9. 70

DOI: https://doi.org/10.1038/s41528-025-00426-3

Publisher: Springer (Nature Research)

Version: Published Version

Downloaded from: https://e-space.mmu.ac.uk/641658/

Usage rights: Creative Commons: Attribution 4.0

Additional Information: This is an open access article published in Npj Flexible Electronics, by Springer (Nature Research)

Data Access Statement: All data generated or analyzed during this study are included in this published article and its supplementary information files. Additional data related to this paper are available from the corresponding author upon reasonable request.

Enquiries:

If you have questions about this document, contact openresearch@mmu.ac.uk. Please include the URL of the record in e-space. If you believe that your, or a third party's rights have been compromised through this document please see our Take Down policy (available from https://www.mmu.ac.uk/library/using-the-library/policies-and-guidelines)

Published in partnership with Nanjing Tech University



https://doi.org/10.1038/s41528-025-00426-3

Low-voltage wearable tactile display with thermo-pneumatic actuation

Check for updates

A. Mazzotta^{1,2}, S. Taccola^{3,4}, I. Cesini¹, M. Sanchez Sifuentes^{3,4}, R. A. Harris^{3,4} & V. Mattoli¹

Tactile displays often face challenges like high power consumption, bulky control systems, and limited portability, hindering their application in wearable technologies. This work presents a novel thermopneumatic tactile display that operates via localized heating of a small air volume, enabling low-voltage operation with standard batteries. Its fully portable design integrates control electronics into a wearable bracelet with Bluetooth activation, enhancing practicality. Mechanical tests demonstrated the device's ability to generate forces exceeding 30 mN and displacements of tens of microns using pulsed signals with modulable durations and frequencies. User tests with voluntary participants confirmed its effectiveness as a tactile display, achieving 83% accuracy in recognizing Braille patterns. By addressing key limitations of traditional systems, this approach offers a promising solution for compact, low-power wearable tactile interfaces.

Haptic interaction is a fundamental process through which humans touch, explore, and manipulate objects. The sense of touch plays a crucial role in our interaction with the external world, providing essential feedback for tasks requiring precision and control. In this context, tactile interfaces have become increasingly important, facilitating interaction with machines and computer systems, improving the controllability of the devices or to reproduce tactile sensations in virtual reality¹⁻⁴. Over the past decades, several wearable tactile displays have been developed, employing diverse actuation strategies to convey tactile stimuli to the human body^{5–10}. These strategies are designed to address different haptic stimuli modalities through specific actuation principles that are suitable for mechanical implementation in wearable haptic devices¹¹. A first and general distinction can be made between mechanical and electrical displays: while the mechanical ones aim to produce a deformation on the human skin by applying a force or a displacement on it, the electrical ones are developed to stimulate the nerves in the human tissues by using electrical current densities in the range 0.1-10 mA cm⁻² 12,13. These latter allow to obtain simplified structures and electrodes that can adhere to the soft tissues of the human body¹⁴. However, electrical stimulation has a strong dependence on skin impedance, which depends on sweating and changes in hydration, making it difficult to maintain constant current injections with the possibility to cause unpleasant sensations or electrically induced lesions⁶. Moreover, since the mechanoreceptors in human skin are sensitive to pressure and displacement, mechanical activation reproduces the true sense of touch, transmitting these changes to the brain via afferent nerves, just as occurs when touching or manipulating an object 15,16.

In recent years, the interest in wearable tactile displays has grown exponentially, aiming to achieve highly flexible, lightweight and portable devices that can be easily worn on different parts of the body¹⁷. To do this, the actuation system must be carefully investigated, in order to avoid the use of large and bulky devices that could significantly affect the mobility of the user. Chen et al. recently reviewed the most commonly used actuation modalities in wearables, pointing out advantages and disadvantages¹⁸. The main drawbacks of such technologies are still represented by their poor portability (pneumatic, hydraulic, and electromagnetic actuators)^{19,20}, high driving voltages (piezoelectric and DEAs)^{21–24}, or hard controllability (Shape Memory Alloys and Polymers, SMA or SMP)²⁵. Within this framework, there is a constant need to explore new implementation strategies that result in displays that are compact, lightweight and energy efficient. Wearable haptic devices are typically studied to be worn on the hands - often in the form of gloves - or on the arms²⁶, or directly on fingers, including ringshaped designs²⁷. Moreover, ideal haptic displays should be imperceptible and unobtrusive until they are activated²⁸. In general, the use of thin films and soft materials allow to reach the conformability needed for following the multiple deformations of the human skin, making haptic displays nearly imperceptible to the user while providing reliable tactile sensations due to their tight contact with the skin^{6,29}. Structural designs and advanced fabrication techniques allow the development of smart platforms that can be directly attached to the user's body. In recent years, different strategies have been proposed for the development of electronic skins by employing different transduction mechanisms. Some examples relate to the possibility of integrating magnets as miniaturized actuators embedded in thin deformable

¹Center for Materials Interfaces, Italian Institute of Technology, Pontedera (PI), Italy. ²The Biorobotics Institute, Scuola Superiore Sant'Anna, Pontedera (PI), Italy. ³Future Manufacturing Processes Research Group, University of Leeds, Leeds, United Kingdom. ⁴Faculty of Science and Engineering, Manchester Metropolitan University, Manchester, United Kingdom. — e-mail: arianna.mazzotta@iit.it; s.taccola@mmu.ac.uk; virgilio.mattoli@iit.it

films, which can be activated through electromagnetic induction to generate vibrations for haptic sensations on the human body^{30,31}. Other fully wearable examples involve the use of electro-hydraulic actuators that incorporate drops of dielectric oils between two electrodes, allowing for the generation of notable normal forces and displacements when activated ^{32,33}.

One of the most accomplished applications of haptic interfaces are Braille displays, although most of the commercial products are not wearable or flexible since they were optimized for desktop-type environments^{34,35}. Visually impaired people use the traditional Braille technique in the fields of education and knowledge, to access written sentences, relying on their tactile sensation to obtain and exchange information. Braille is a tactile reading system that uses arrays of six or eight raised dots (arranged respectively in 3×2 or 4×2 arrays) representing the letters of the alphabet, punctuation marks, numbers, and symbols characters^{36–38}. To date, different refreshable Braille displays -i.e. displays capable of dynamically update Braille characters over time-38,39 have been proposed40-44. Noteworthy, this technological solution can be employed to realize larger arrays of dots, in addition to the standard 3×2. Having a higher number of active dots could be useful for displaying more complex information and dynamic patterns, such as motion sensations, complex characters, properties of the handled object such as its shape and dimensions, and navigation instructions ^{6,32,34,45}.

In this work, we present a wearable thermo-actuated device capable of providing vibro-tactile sensations to the human body (Fig. 1). The working principle of the device is based on an electrically controlled thermopneumatic actuation that exploits the expansion of a closed small volume of air thanks to a very localized increase in temperature. This approach has been previously investigated by the authors in a preliminary study based on an ultra-thin tattooable device with different levels of conformability, materials, and thicknesses, where, however, only one "taxel" - i.e. tactile pixel - has been validated on the human fingertip⁴⁶. The tactile display presented in the current work brings several updates such as higher reliability and robustness, as well as the possibility to control the volume of air through the dimensions of the chamber, in addition to the demonstration of a larger and more advanced device. A key enabler in these updates was the ability to fabricate the novel tactile display by using a bespoke computercontrolled Aerosol Jet Printing (AJP) system^{47,48}. We found in literature very few examples regarding the implementation of thermo-pneumatic devices based exclusively on the air expansion. Similar concepts have been applied across different domains and different scales, developed for example as artificial muscles⁴⁹, tip-tilt-pistons⁵⁰, pumps and microfluidic systems^{51,52}, or actuators^{53,54}, but, to the best of our knowledge, not as wearable tactile displays. Examples of Braille displays featuring thermo-pneumatic actuation often include the use of air chambers beneath the region devoted to the active dots and/or external compressors for air inflation, thereby reducing the portability of the device 19,23,55,56. Some tactile displays also use working liquids heated by underlaying heating elements, leading to thicker final devices that are not easy to integrate on wearable platforms ^{57,58}.

Compared to other technologies such as pneumatic or hydraulic actuators, the display proposed here does not need the presence of further bulky components such as reservoirs, valves or pressure tubes or sources. This aspect helps to improve the conformability, lightness, and portability of the device itself. Noteworthy, the tactile display presented in this work can be entirely realized by additive manufacturing techniques and the considered steps can be easily scaled up and/or integrated using well-known prototyping manufacturing processes like standard flexible PCBs, as demonstrated later in this paper.

Results

Thermo-pneumatic actuation: overview

We refer to thermo-pneumatic actuation as the working principle on which the proposed tactile display is based⁴⁶. The approach used in this present work is schematically depicted in Fig. 1a: a flexible Kapton HN Polyimide thin film is used as the substrate on which a resistive element is printed as the heater and, in correspondence to it, a holed Kapton spacer and a deformable

Polydimethylsiloxane (PDMS) membrane placed on top are used to create an enclosed volume of air (0.044 mm³) – components depicted in Fig. 1b. Once the resistor is powered, the air expansion due to Joule heating causes the movement of the thin PDMS membrane on top, thus leading to the possibility of generating forces once the device is put in contact with a substrate – i.e. the human skin. A schematic illustration of the fabrication process used for the manufacturing of the tactile display is reported in Fig. 1c and described in detail in the Experimental Section. Concerning the materials used, Kapton is well known for its excellent thermal stability at high temperatures. The thermal conductivity of Kapton is 0.8 W/(m·K): using a film with low thermal conductivity allows a limited dispersion of heat, thus concentrating the heat in the air chamber for a more efficient increase in temperature. PDMS was selected for the top movable membrane primarily due to its well-known capability for oxygen plasma bonding, which allows secure attachment of two PDMS layers. This step was critical for the realization of a closed volume of air (step 5 in Fig. 1c) confined between the Kapton film, the Kapton spacer, and the top membrane, ensuring no air leaks during activation. Notably, PDMS has been extensively studied and widely used in biomedical applications. However, in future studies, it could potentially be replaced with more elastic materials, such as Ecoflex. Noteworthy, we decided to use thin printed conductive traces as resistors instead of wires or coils, mainly because of their ultra-thin thickness. The printed tracks have a low thermal capacity, thus allowing a fast response during Joule heating and cooling, avoiding a potential limit in the activation frequency. The resistors were printed using a bespoke computercontrolled Aerosol Jet Printer (AJP) apparatus. AJP is an emerging contactless direct write technology with distinct advantages in terms of fastprototyping, wide ink compatibility and a printing resolution of the order of 10 μm, enabling the manufacturing of high-resolution features over a variety of flat and three-dimensional surfaces, different surface textures, across curved surfaces, and into channels 47,48. Thanks to these unique properties, AJP is increasingly used in the manufacturing of miniaturized actuators, sensors, and components used in active and passive wireless technologies and other microelectronic devices, for a wide range of applications, including healthcare and conformal electronics^{59,60}. In this work, AJP was used for high-precision printing of resistors with unprecedented resolution compared to our previous work.

Before the implementation of the first prototype, a finite element model – reported in ref. 61. – was performed in order to investigate the thermopneumatic activation principle and understand if it could be exploited to develop wearable transducers. Preliminary simulation results showed that the displacements of the flexible membrane and the force generated by air expansion - achieved by using various activation signals corresponding to specific temperature dynamics - were found to be satisfactory for reproducing vibro-tactile sensations on the human fingertip. As a further implementation, the presented model can be easily adapted by modifying its components and/or materials. For example, we incorporated a glass slide to simulate the substrate on which the display was placed (Supplementary Fig. 1), replicating the experimental conditions, particularly with respect to thermal dispersion throughout the substrate. More details about the simulation results are discussed in Section "Advanced Prototype".

Along this paper, two designs for the tactile display are presented. The first prototype showed was used to validate the thermo-pneumatic activation strategy for the realization of tactile displays (Fig. 1d). Based on these results, we implemented a second design, to create a fully wearable platform and conduct tests on voluntary subjects (Fig. 3a). The first prototype was entirely produced on Kapton thin films and conductive traces made by AJP, while the second one has the same fabrication strategies and working principle but was built on a specifically designed flexible PCB to facilitate connection between the display and the rest of the electronics. Despite the different characteristics of the two devices, the size and number of dots of the single cells are the same (1.5 mm diameter), based on the standard dimensions of Braille displays (dimensions reported in Supplementary Fig. 1)^{58,62}. As designed, the proposed transduction strategy can be easily integrated into

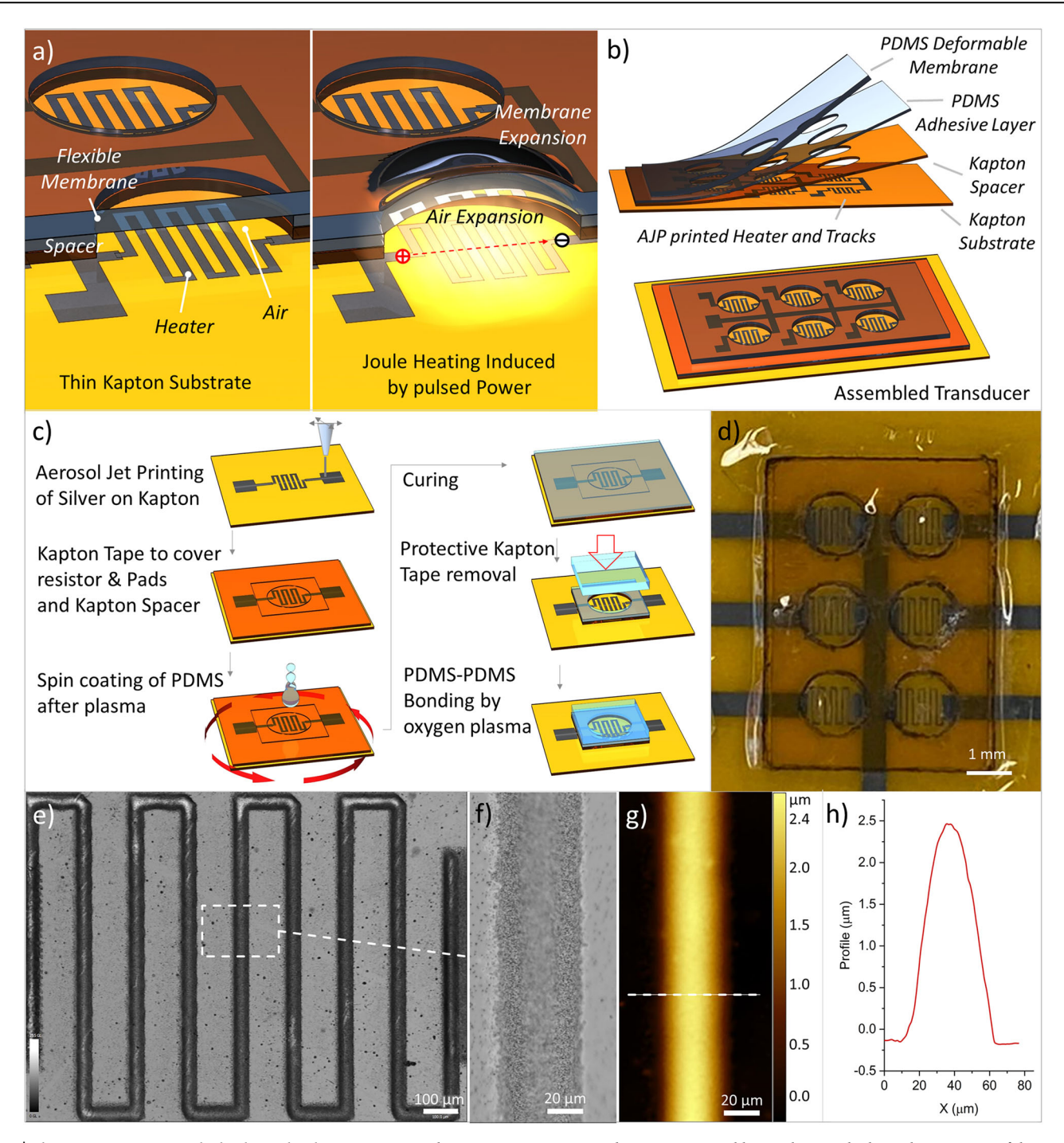


Fig. 1 | Thermo-pneumatic tactile display technology overview. a Thermo-pneumatic actuation strategy used to activate display taxels and b structure of the tactile display; c Schematic of the fabrication process used for the manufacturing of the display; d Optical image of the first developed prototype made by resistors printed by using silver nanoparticle ink directly on Kapton film, a holed Kapton

spacer, and top PDMS movable membrane; ${\bf e}$ high-resolution image of the serpentine resistor with ${\bf f}$ magnified view of a single printed line, and ${\bf g}$ correspondent confocal profilometry image. ${\bf h}$ Printed line thickness profile, corresponding to dash line in ${\bf g}$, showing a maximum thickness of about 2.4 μ m.

wearable and portable devices. For this reason, we then tried to move the device for possible large-scale production, integrating our fabrication strategy with standard fabrications such as flexible PCB manufacturing.

Device characterization

Morphological and Electrical Characterization - The resistor used in this work had a serpentine shape as shown in Fig. 1e (see also Supplementary Fig. 1). The shape and dimensions of the heater inside the air chamber were designed in such a way to achieve uniform heating inside the actuation

chamber. Thanks to the high resolution of the aerosol jet printer, it was possible to obtain fine features – reaching line widths ${\sim}55~\mu m$ – that presented a good level of conductivity. According to optical profilometer measurements, the maximum thickness of the printed serpentines was $2.2\pm0.3~\mu m$ (see Fig. 1g, h for single example and Supplementary Fig. 2 for statistics). The design dimensions and the printing parameters were chosen also to obtain a good level of conductivity of the resistors: a resistance of $27\pm9~\Omega$ - average and standard deviation on a total of 60 printed serpentines- was achieved.

Thermo-Electrical Characterization - First, the temperature trends of the printed resistors were tested through a thermal camera. The resistor considered was activated with 1 W nominal peak power. The temperature reached by the resistor is reported in Fig. 2a: different pulse durations were investigated, equal to 10, 25, 50, and 100 ms. The thermal images in Fig. 2a point out how the increase in heat is localized at the level of the activated dot for every pulse width considered. One dot of the final fabricated device was tested in air under the thermal camera for different activation signals. In particular, different Pulse Widths (PW), Frequencies (F) and thus Duty Cycles (DC) were considered by applying a peak power excitation of 1 W. Signals considered were: PW: 10 ms, F: 1 Hz, APW 10 mW; PW: 25 ms, F: 1 Hz, APW 25 mW; PW: 10 ms, F: 2 Hz, APW 50 mW; PW: 10 ms, F: 10 Hz, APW 100 mW, where APW is the average power of the actual applied signal. The temperature trends of these signals are reported in Fig. 2b (with a detailed zoom of the initial activation on Fig. S3a), showing how temperature values coherently follow activation pulses, made exception for the last reported signal (PW: 10 ms, F: 10 Hz) since the frequency of the signal was higher than the acquisition frequency of the thermal camera (9 Hz). As expected, the average temperature (averaged on a circular region of interest surrounding the dot) increases with increasing frequency of the signal.

Despite the reached values resulted quite high, once the device is put in contact with a material with a higher heat capacity – i.e. the human skin - the maximum temperatures are lower and the user should not perceive the generated heat, as also confirmed by the experimental tests on subjects (see Section "Advanced Prototype"). The sequence of thermal images in Fig. 2b and Supplementary Fig. 3b (where different time intervals for the same signal are considered) show how the temperature increase was localized at the level of the tested taxel and the heat was rapidly dispersed with each pulse in all the time steps considered ((i) –(iii) in Supplementary Fig. 3).

Actuation performances

The normal force exerted, and the corresponding normal displacement were analyzed by activating the display dots using various signal types. During testing, the power was carefully adjusted to achieve a nominal peak power output of 1 W. The measured values were used as clear benchmarks for the device's performance and provided reference data for evaluating repeatability, both within a single device (intra-device reproducibility) and across multiple displays (inter-device reproducibility). Specifically, the oscillation amplitude and the average values of force and displacement were considered for all the activation signals. The meaning of these values is reported in the representative force and displacement signals in Fig. 2c, f. For the evaluation of the oscillation amplitude, we considered the height of 10 peaks for each signal and for each of the 6 dots in the time interval 10-20 s so as to obtain mean values and standard deviations for the different signals, reported in Fig. 2d, g, respectively for force and displacement. Concerning the average force and displacement, we considered the overall average values obtained during the acquisition time; mean values and standard deviations for the different activation signals are reported in Fig. 2e, h, respectively for force and displacement. The signals reported are indicators of the intra-device reproducibility in terms of the force/displacement oscillation amplitude and mean force/displacement. Each colored dot represents the mean values and standard deviations of the oscillation amplitudes of each of the six dots of the display. As expected, the highest force oscillation amplitude was found for the signal with longer pulses (25 ms-1 Hz). In this case, the mean value of force was ~5 mN, corresponding to a pressure of 2825 Pa. The pressure was calculated as the ratio between the obtained (normal) force and the area of the dot (1.77 mm², since the diameter is 1.5 mm, see Supplementary Fig. 1 for the dimensions). The minimum difference in pressure was observed in the peaks related to 10 ms-10 Hz signal, corresponding to ~1100 Pa. The force response corresponding to the activation signal 10 ms-10 Hz showed low oscillation amplitude but the largest values of the mean force. These results show a decrease in oscillation amplitude with increasing frequency, probably due to thermal inertial effects becoming more important.

The same analysis about intra-device reproducibility was performed in terms of the achievable displacement. A representative signal is reported in

Fig. 2f, with the values considered as indicators – i.e. displacement oscillation amplitude and average displacement. The mean values and standard deviations of the intra-device reproducibility measurements in terms of achievable displacement are reported in Fig. 2g, h. Approximately the same trends observed for the force response were found also for the displacement. Notably, in the case of the 10 ms–10 Hz activation signal $\sim\!\!6\,\mu m$ of mean displacement were achieved (Fig. 2h).

We conducted a parallel investigation to evaluate inter-device reproducibility. For the assessment of force and displacement oscillation amplitude, we applied the same methodology used for assessing intra-device reproducibility. Specifically, we averaged the data obtained from ten 'central' peaks of force and displacement recorded at various activation signals across five different devices, resulting in a total of five data points per signal. For the mean force assessment, we computed the average of all signals measured at various activation powers across the five different devices, considering the entire duration of the test. The obtained mean values were averaged again, and standard deviation was obtained from them. The mean values of both the force and displacement (Supplementary Fig. 4b, d) were slightly lower compared to the previous tests, especially in the case of 10 ms-1 Hz and 25 ms-1 Hz signals. Nevertheless, mean pressures obtained were in the range 329-4237 Pa (0.7-7.5 mN) and mean displacements of almost 2 μm, at a nominal peak power of 1 W. The force and displacement oscillation amplitudes are reported as inter-device reproducibility indicator (Supplementary Fig. 4a, c): only one device presented less than 1 mN force oscillations, while all the others achieved more than 1 mN and more than 1 μ m.

The averaged signals of force and displacement obtained by averaging over time and over the 5 tested dots of the 5 devices are shown in Supplementary Fig. 5, for all the activation time and with a zoom on 1 s acquisition time interval. These results indicate some variations in performance among the devices, with some exhibiting lower performance compared to others.

As a final test for this prototype, the force signal was measured for one week, showing that the force values were stable all over the 7 days (Supplementary Fig. 6).

The characterization tests showed that the developed actuator exceeded the tactile perception threshold found in the literature⁶³. On average, the tactile perception threshold is related to the frequency of the vibro-tactile signal used: vibratory inputs correspond to lower thresholds for eliciting a tactile sensation, compared to static deformations, and, even when vibrotactile amplitude is not changed, the perceived intensity can increase as the frequency increases^{34,64,65}. For example, at a signal of 5 Hz the force threshold at the fingertip is 4 mN, while at 250 Hz it decreases to 2.2 mN⁶⁶. Concerning displacement, the lowest threshold at the fingertip, 0.02 μm , has been found at a frequency of around 200 Hz⁶⁷; in another study, Lindblom, using halfcycle sinusoidal mechanical pulses through a cylindrical indenter, reported a detection threshold of 5 µm for stimuli inducing rapid skin displacements, down to 0.3 mm/sec (on the order of 10 Hz), which rapidly increased to tens of microns for slower stimuli⁶⁸ (for comparison, the rate of displacement in this study is in the order of 0.6-0.8 mm/s, mostly independent from the pulse duration applied). The variation of threshold detection is due to the different sensitivity of the mechanoreceptors of the human skin to different stimulation frequencies 68.

Advanced prototype

Although even relatively lower performing devices achieved satisfactory force levels at the applied powers, the preliminary experiments revealed significant variability among the tested samples. The continuous heating of the resistor can, over time, alter its resistance value. This occurs because the nanocomposite ink used for AJP (annealed/sintered at 200 °C for 10 min) can undergo further sintering due to the Joule heating effect during transducer operation. When driven by a voltage source, the resistor value should be monitored to adjust the excitation voltage accordingly, ensuring that the delivered power remains constant. To address this issue and ensure reliability in wearable applications, a custom electronic circuit has been designed and developed. This circuit can deliver a precisely settable constant power, including the ability to operate in a pulsatile mode with high precision. The

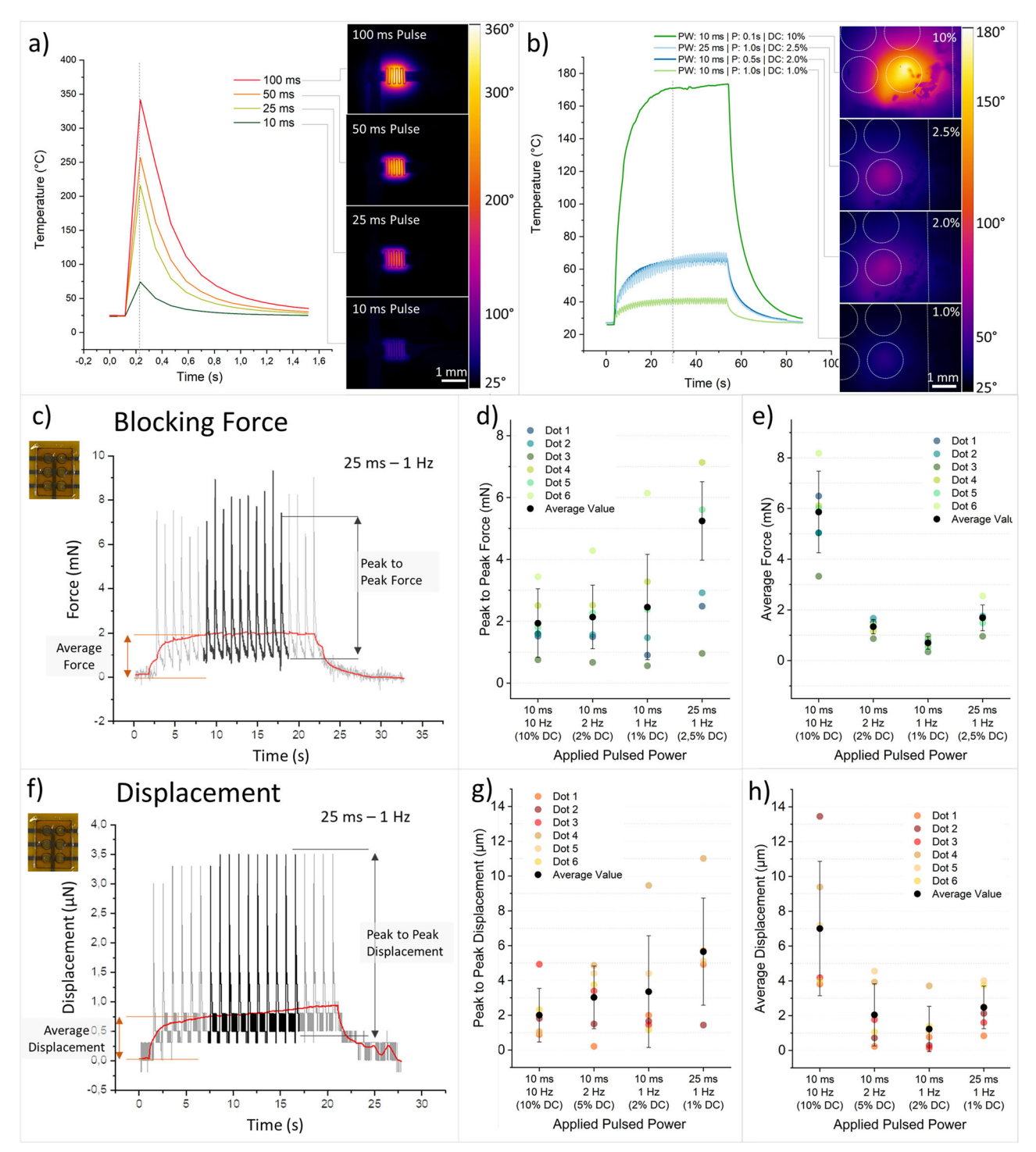


Fig. 2 | Thermo-electrical characterization of tactile display first prototype. a Temperature response of the resistor with different pulse durations of activation signals (temperature has been measured on Kapton surface in the middle of the heater, between two tracks of the serpentine) and thermal images of the resistor taken at the time step corresponding to the peak of temperature for every activation signal; b Temperature dynamics of the complete fabricated device at different activation signals (PW 10 ms- DC 1%, PW 10 ms- DC 2%, PW 25 ms- DC 2.5%, PW 10 ms- DC 10%) with 1 W peak power: the reported thermal images of the activated dot for each activation signal has been acquired after 30 s from the start of the activation; c Force characterization. Representative signal obtained by force measurements that shows the parameters used for characterizing the device: the average force exerted and the amplitude of the force oscillation generated by the pulsed signals (averaged on 10 central peaks for each dot and each activation signal); d Mean values and standard deviations of the force oscillation amplitude (in black)

exerted by each of the 6 dots of one display at the different activation signals (single values reported as colored dots in the graph) and ${\bf e}$ average values and standard deviations of the average force (in black) from the 6 tested dots for each activation signal (each value reported as colored dot); ${\bf d}$, ${\bf e}$ Represent the intra-device reproducibility; ${\bf f}$ Displacement characterization. A representative signal obtained by measurements on the displacement (in ${\bf \mu}{\bf m}$) that shows the parameters used for characterizing the device: the mean displacement achievable and the amplitude of the displacement oscillation generated by the pulsed signals; ${\bf g}$ Mean values and standard deviations (in black) of the displacement oscillation amplitude shown by each of the 6 dots of one display at the different activation signals (single values reported as colored dots in the graph) and ${\bf h}$ mean values and standard deviations of the average displacement (in black) from the 6 tested dots for each activation signal; ${\bf g}$, ${\bf h}$ Represent the intra-device reproducibility in terms of obtained displacement.

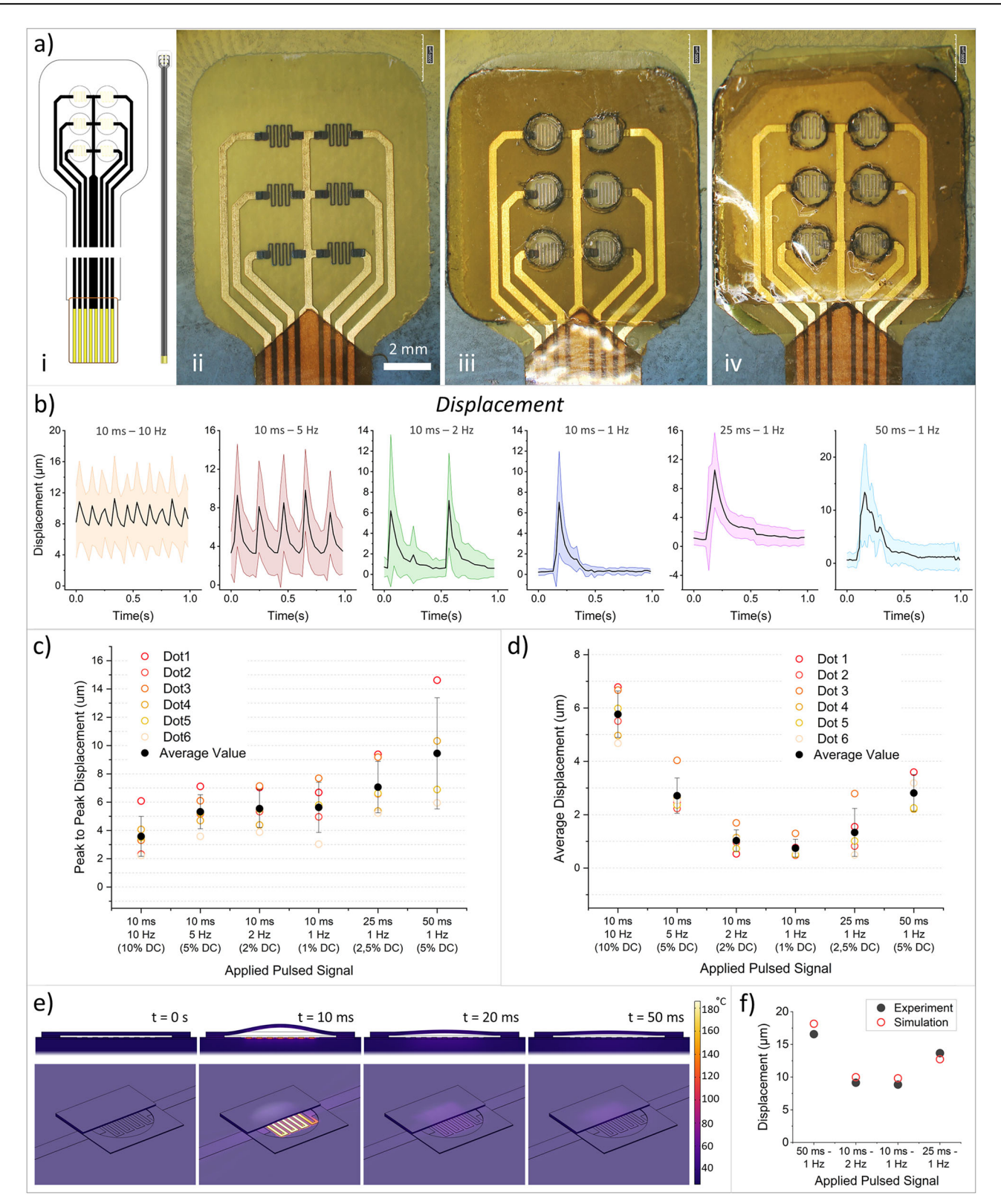


Fig. 3 | Advanced prototype design and displacement characterization. a Layout of the new prototype used for the development of the flexible PCB in outsourcing (i) with the real fabricated one (ii) on which the silver nanoparticle ink resistors were printed to connect the conductive traces and obtain a localized increase of temperature in correspondence of each taxel; the holed Kapton spacer (iii) and the movable PDMS membrane (iv) were added to obtain a fully-working tactile display; b Inter-device reproducibility. Displacement values averaged in time on 5 dots chosen from 5 different displays, reported as mean values (black line) and standard deviation (colored edges) for each activation signal tested. All the experiments were

conducted with 1 W peak power (complete signals reported in Supplementary Fig. S9b); \mathbf{c} , \mathbf{d} Intra-device reproducibility. Characterization of the new prototype with the same figures explained in Fig. 2 and Section "Device Characterization". \mathbf{e} Frontal and 3D section view with temperature plot from the finite element simulation for the displacement investigation in the case of 10 ms pulse (the displacement in the frontal view section was magnified of 10 times so that the overall movement is clear); \mathbf{f} maximum displacement (peak values) reached in simulation and experiment (average peak values of the displacements on the five tested displays).

wearable power control board (see Fig. 5a with the schematics and layout reported in Supplementary Fig. 7) is fully wireless and allows for the generation of complex pulse patterns on demand via a dedicated software interface developed specifically for this purpose (see sections "Haptic demonstration on subjects" and "Experimental Protocol", and Supplementary Fig. 7). The nominal power can be easily adjusted via the user interface by modifying the current settings, as illustrated in Supplementary Fig. 8.

We adopted a hybrid approach in the vision to use the portable electronic board with our device, by integrating the previously explored fabrication strategy and actuation principles with standard techniques, such as the use of flexible PCBs. These latter enabled direct connection of the display to the electronic board via appropriate connectors, facilitating the implementation of constant power control (which details are given in the section of the Methods dedicated to the Portable Electronics Layout). The layout used is schematically shown in Fig. 3a.i and the fabrication was carried out by using standard flex PCB fabrication processes (see Supplementary Information). The Au-Cu traces of the flex PCB were connected by the direct printing through AJP of the same serpentines showed in the previous prototype, in order to create the six independent taxels. It is noteworthy that the high flexibility and scalability offered by AJP technology allows the number and design of printed traces to be easily changed, providing for the manufacturing of more complex, larger and personalized tactile displays. The sequence of optical images reported in Fig. 3a.ii-iv illustrates the steps of the fabricated second prototype. It is possible to carry out two steps in parallel: on one side, printing the resistors on the flexible Kapton, and on the other, fabricating the Kapton spacer with the bonded PDMS membrane, which will later be transferred and attached to the flexible PCB. Specifically, the Kapton spacers are coated with a thin layer of PDMS via spin coating immediately after laser cutting (which creates the circles for trapping the air volume), allowing the PDMS movable membrane to be bonded using oxygen plasma. Notably, the circles for the air volume are not filled with PDMS, as the laser cutter parameters are carefully adjusted to avoid completely removing of the circular sections during cutting. Instead, these sections are designed to be removed only after the spin coating and curing of the thin PDMS layer, before bonding the membrane. Sealing is a crucial factor in the fabrication of the device. To achieve good adhesion, we polymerized the thin layer of PDMS spin-coated on top of the Kapton spacer before proceeding with plasma bonding of the PDMS membrane. While the chosen approach has proven to be sufficiently reliable for this demonstrative application, alternative methods – such as SiO₂ mediated bonding, nitrogen plasma treatment, sputtering in an Ar⁺ ion plasma, or chemical functionalization of the surfaces - could be explored to further enhance the adhesion between Kapton and PDMS 69-72.

The same mechanical characterization considered for the first prototype was carried out for the second one. During these tests, the samples were connected to the customized electronic board to have controlled power for the activation. Moreover, two more signals for the activation were considered, corresponding to 5% Duty Cycle (DC) - i.e. 10 ms PW 5 Hz and 50 ms PW and 1 Hz. As reported in Figs. 3b-d and 4a-c, the new display demonstrated significant improvements in term of both measured force and displacement, compared to the previous prototype, largely exceeding the vibro-tactile perception thresholds. The intra-device reproducibility tests, presented in Figs. 3c, d and 4b, c, revealed trends consistent with those observed in the initial prototype. Among the activation signals, the 10 Hz signal once again exhibited the highest response in terms of both average displacement (Fig. 3d) and average force (Fig. 4c). The displacement values were comparable between the two prototypes, whereas the average force achieved with the new prototype were more than doubled, increasing from approximately 6 mN in the previous experiments to around 13 mN. This enhanced performance was also observed in force oscillations, where pulses of 25 ms at 1 Hz and 50 ms at 1 Hz reached forces of 20 mN (11 kPa) and 33 mN (18 kPa), respectively. Regarding the inter-device reproducibility (all graphs reported in Supplementary Fig. 9, and complete signals reported in Supplementary Fig. 10), the standard deviations obtained from these second prototypes - especially in the case of the force - resulted to be lower compared to the previous tests, clearly indicating an improvement in the controllability of the driven signals applied on each dot, even on the five different displays. High frequency acquisition test (20 kHz sampling frequency) revealed the possibility to achieve peak forces of 5, 10, 15, 20, and 30 mN even with single pulses of different duration (5, 10, 25, 50 ms, Fig. 4d). All the tests described earlier were conducted at a nominal peak power of 1 W. A sweep of the activation power, ranging from 0.5 to 1.1 W, demonstrated that an average force exceeding 2 mN can be achieved even at the lowest power when using a 10 ms–10 Hz signal (Fig. 4e). This power sweep was further investigated during experimental tests with voluntary subjects, as it provides valuable insights about the thresholds for touch perception.

The achieved displacement values showed excellent agreement with those obtained during simulations, as detailed in Fig. 3e, f, both in terms of maximum displacement - peak values of the average displacement and peak values from simulation - and dynamic relaxation, as reported in Supplementary Fig. 11. This aspect highlights the robustness of the finite element model for further investigations of materials and geometry in the vision of optimizing this platform.

Overall, significant values of forces and displacement were generally obtained both in the case of the oscillation amplitude analysis and the mean values, with an improved response observed in the case of the second prototype. The mechanical characterization suggested the versatility of the display which could be used for eliciting a wide range of sensations, from more static to dynamic ones, by changing the parameters -i.e. PW and frequency – of the activation signal.

Given the values achieved in terms of force and displacement, it was therefore assessed that the thermo-pneumatic actuation strategy proposed here can be exploited for the realization of tactile displays. Specifically, the second prototype proposed can be easily integrated with custom designed portable electronics, which ensures higher controllability on the activation of the single taxel, resulting also in enhanced performance of the display. From the characterization emerged that the activation signal 10 ms–10 Hz showed the widest response in terms of average force, as well as the lowest standard deviations in all the conducted tests, showing less possibility of variability among different samples. Consequently, this signal was used during tests on subjects.

Haptic demonstration on subjects

To further investigate the possibility of using the display for providing tactile sensations on human skin, we performed experimental tests on healthy subjects. The portable electronic board specifically developed for this application (Fig. 5a) was integrated into a bracelet so as to enhance the wearability of the platform during the tests (Fig. 5b). More details about electronics are given in the Materials and Methods and Supplementary materials. During the tests we decided to attach the device to the index fingertip of the subject by using Tegaderm Medical Tape to ensure good adhesion of the device to the fingertip. Moreover, a thin metal plate on the back of the device, under the active dots, allows to increase local rigidity and favorite thermal dissipation. The testing protocol is based on the activation of the dots with different patterns, and it is divided into 3 steps, schematically reported in Fig. 5c. The first step of the protocol is useful to determine if the subject can discern the activation of the same dot or of two different dots close-by, in the "near" activation, or "far away". During the second step we wanted to investigate more the possibility of distinguishing dynamic patterns, like the upside or downside movement, as well as clockwise and anticlockwise activations. The third and last step of the test regards the possibility that the subject recognizes which letter of the fixed range A, I, L, O, T, V (in Braille alphabet) has been activated. These 3 steps focus respectively on determining the threshold of perception for two-point recognition, threshold of perception for dynamic patterns, and, finally, the success rate in recognizing specific characters. In the final section of the test, Braille characters were reproduced by sequentially activating the corresponding dots. Each dot during the representation of one character was activated for 5 repetitions before moving to the next, with a total activation time of 500 ms per dot (activation signal 10 ms PW, 10 Hz frequency). This

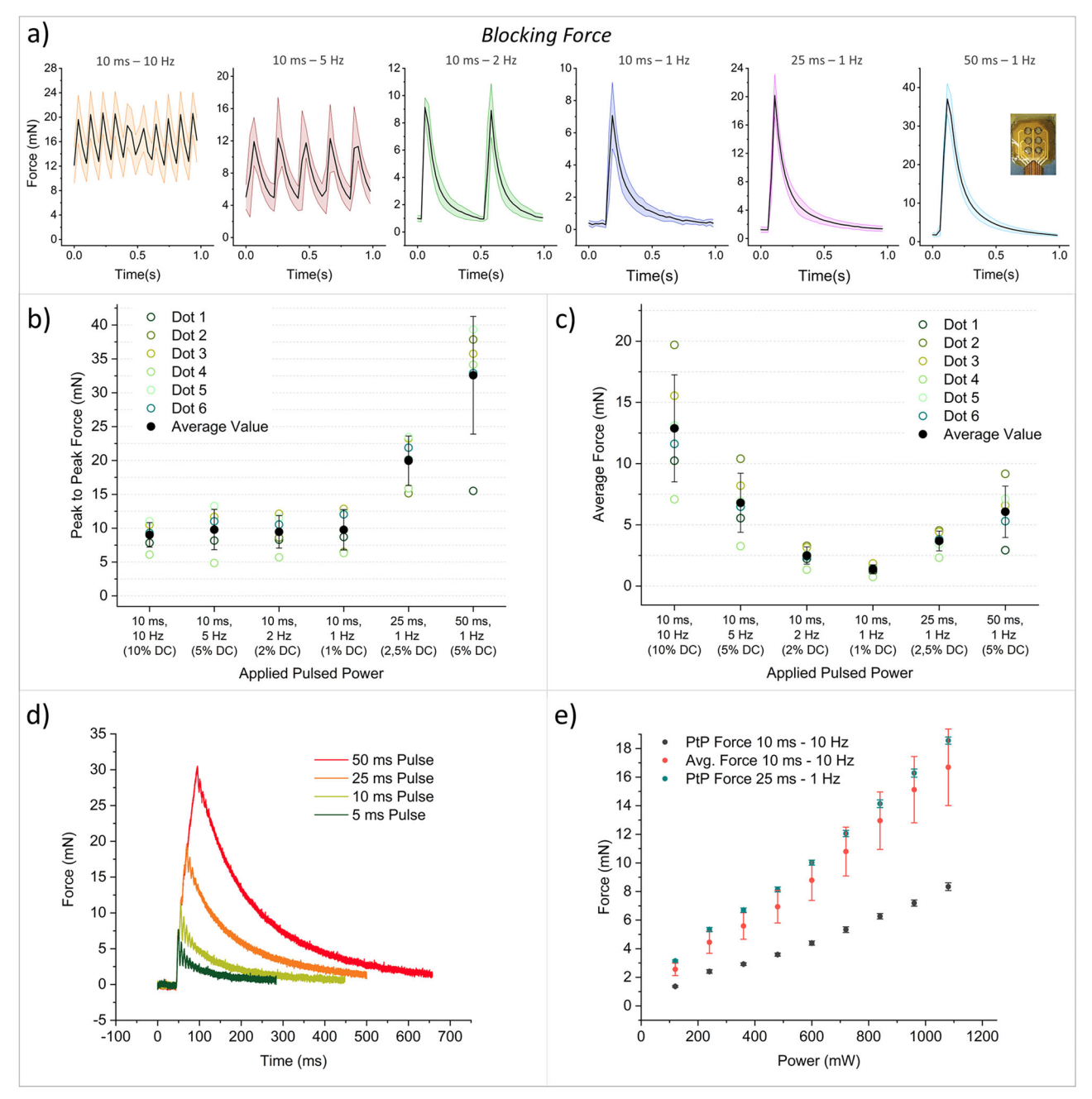


Fig. 4 | Advanced prototype force characterization. a Inter-device reproducibility in terms of exerted force. Force values averaged in time on 5 dots chosen from 5 different displays, reported as mean values (black line) and standard deviation (colored edges) for each activation signal tested. All the experiments were conducted with 1 W average power (complete signals reported in Supplementary Fig. S9a); b, c Intra-device reproducibility in terms of exerted force. Characterization of the

new prototype with the same figures of merit explained in Fig. 2 and Section "Device Characterization". **d** Force response at different pulse durations of the activation signals – acquisition frequency 20 kHz filtered with a moving average over 4 points. **e** Peak to peak and average response of the force in the case of 10 ms–10 Hz and 25 ms – 1 Hz activation signal, with a power sweep from 100 to 1200 mW.

procedure, as illustrated in Fig. 5d and Supplementary Figs. 12, 13, ensured a precise representation of the Braille patterns. The sequence of thermal images in Supplementary Fig. 12 gives an example of how it is possible to replicate some characters of the Braille alphabet on the display (3×2 taxels) by sequential activation of each dot. No crosstalk is observed even during the activations of consecutive taxels.

Perception tests were performed on 10 participants (5 females and 5 males, average age 34 years), after obtaining their informed consent and according to ethical committee authorization (as obtained from Comitato Etico Territoriale Liguria, protocol INPH23). Throughout the duration of

the test, the subject was required to click on the buttons of the dedicated interface (shown in Supplementary Fig. 14) which pattern he/she perceived.

A summary of the results for the two-point recognition and dynamic patterns recognition is reported in Fig. 5e, f. In these two cases, seven levels of nominal peak power were considered for the activation of the device, to detect a possible threshold for the vibro-tactile perception. The average percentage of correct identification is 82% and 85% respectively in the case of the two-point recognition and dynamic recognition, that increases to 89% if we exclude the lowest tested power. Notably, no significant changes in the correct response were detected while decreasing the nominal power, until

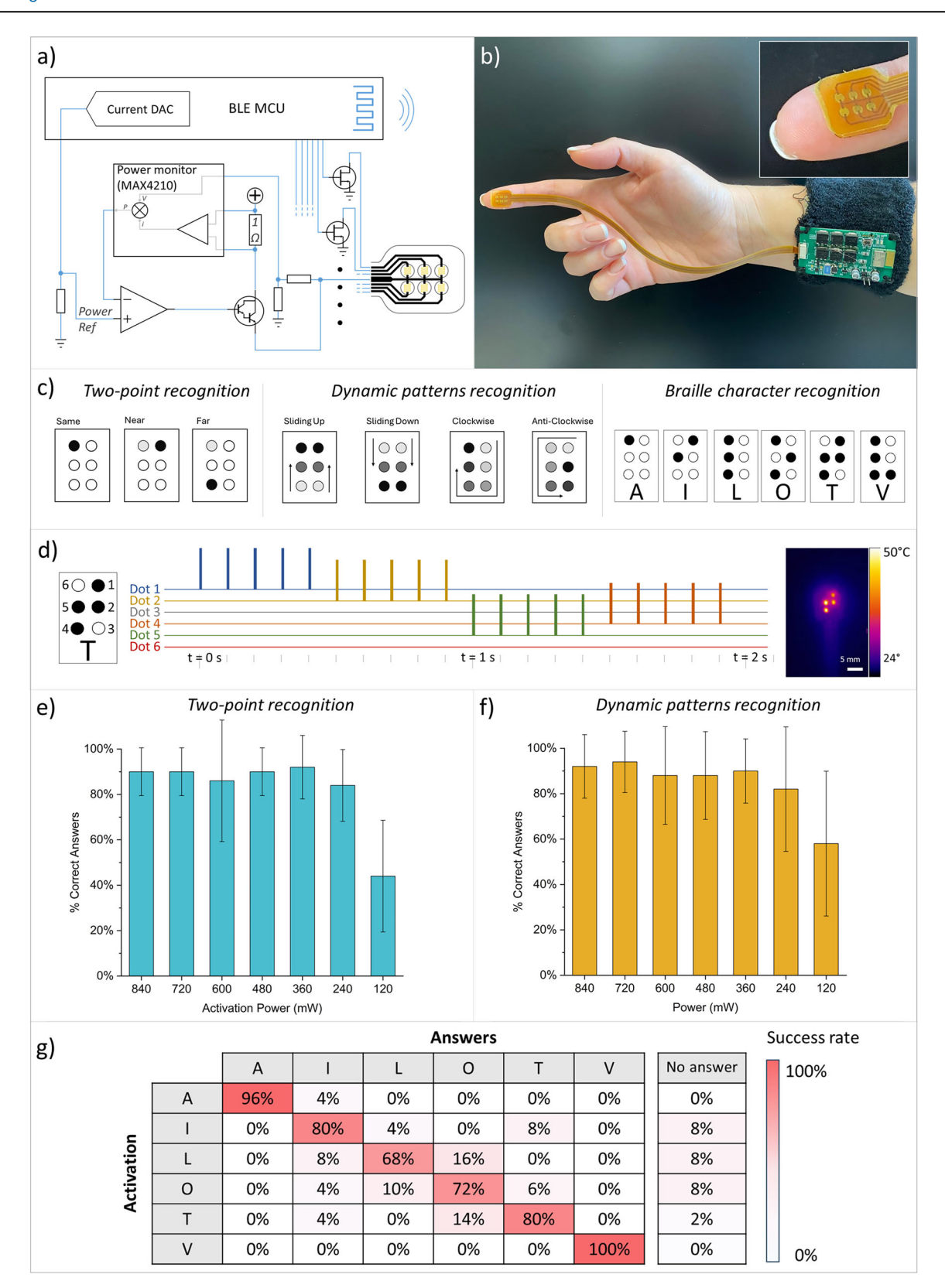


Fig. 5 | **Wearable tactile display demonstration on subjects. a** Schematic diagram of the control system, whose main components are the operational amplifier for closed-loop control of power through the power monitor MAX4210 and wireless communication system; **b** complete wearable platform with the electronic board integrated into a bracelet and the tactile display attached to the fingertip of the user; **c** representation of the three steps used for the tests on voluntary subjects and relates patterns; **d** example of sequential activation of four of the six dots of the tactile

display for reproducing the Braille character "T" (each dot active for 500 ms, since the activation signal was 10 ms-10 Hz), with thermal image made by merging 4 thermal images – one for each active dot – to recreate the pattern of "T"; **e**, **f** Percentage of correct answers averaged on the 10 subjects, respectively for the two-point recognition test and dynamic pattern recognition test, with an average success rate of 82% and 85%; **g** Braille character recognition confusion matrix in the case of 840 mW nominal peak power, where a success rate of 83% was achieved.

the lowest nominal peak power of 120 mW. This aspect underlines the ability of the tactile display to reproduce effective tactile sensations at the different intensity levels. In the case of 120 mW, the two-point recognition patterns were more difficult to distinguish compared to the dynamic ones – where the correct identification was more than 50% - suggesting that dynamic pattern can be better recognized even at lower powers. At a nominal activation power of 240 mW, the standard deviation — particularly in the case of dynamic pattern recognition — is relatively high, indicating significant variability in performance across subjects, with some achieving excellent results while some others performing less effectively. Consequently, the threshold for reliable perception can be identified at a nominal peak power of 360 mW.

The confusion matrix reported in Fig. 5g summarizes the data of the last perception test from all the subjects, regarding the recognition of Braille alphabet characters. This test was performed with two levels of nominal peak power, the highest one (840 mW) and an intermediate one (480 mW), slightly higher than the power related to the perception limit. For each power, 30 random patterns were presented to the subjects, repeating each letter randomly 5 times. The overall success rate of the test with the highest power is 83%, showing the efficacy of the device to provide information through dynamic patterns. Two characters - A and V - were above 90%, while confusion mainly occurred among letters L and O, probably because of the similarity between the two patterns, indicating that longer training may be beneficial. From literature, the Braille characters T and V appear to be commonly confused with other letters, and in relation to our set of characters, T and I are often confused between them⁷³. Noteworthy, we reported a success rate of T and V of the 80% and 100%, respectively, with only 4% confusion of the T character with I. On the base of this observation, we believe that the ad-hoc sequential activation of the dots is a promising way to produce even more robust character recognition. In the case of lower power (confusion matrix in Supplementary Fig. 15) we observed a decrease in performance to a success rate of 75%, which nonetheless remains within an acceptable range. In this case, the percentage of No Answers was higher compared to the previous test, and more confusion was observed especially among the letters L, O, and T, suggesting a lower level of perceptibility of the activated dots.

All subjects were given a questionnaire regarding the level of wear-ability of the display, the type of sensation experienced, and the comfort during the tests to assess the device's user satisfaction. Based on the questionnaire, the display was fully accepted by the users in terms of lightness, bulkiness, and wearability. Notably, none of the participants reported experiencing hot sensations during the tests. The predominant sensation reported was described as a "touch/pressure" feeling.

Discussion

In this work, a flexible and wearable display has been presented. The results obtained from the characterization clearly showed that the display can provide tactile sensations with forces and displacements that exceeded the tactile perception threshold. Overall, the obtained outcomes met the requirement of exceeding the tactile sensation thresholds of 4 mN for the force and 5 μm for the displacement, with exerted forces that reached more than 30 mN peak values and displacement above 10 μm . From the characterization it also emerged that based on the type of signal, it is possible to stimulate the human body in a more static or dynamic way (e.g., vibrations), extending the possibilities of tactile stimulation.

The chosen materials and manufacturing process enabled precise control of the enclosed air volume, leading to high levels of reliability and reproducibility of the technique. The tactile display presented in this work encompasses several advantages of other devices in the literature (summarized in Supplementary Table 1 for comparison). The main aspects are related to high wearability, possibility to adjust the taxels pitch – with the possibility to reach high resolution to obtain a wearable array on the fingertips, as well as the use of consolidated fabrication technologies, enabling the scalability and the potential low cost of the device. More in details, the device is activated with low voltages and thus can be easily powered by

batteries and integrated with a Bluetooth control module, enhancing the level of its wearability. Furthermore, the second prototype reported in this work could be easily integrated into gloves or fabrics to make it adherent to the subject's hand. The fabrication process used involves techniques such as the aerosol jet printing of conductive inks, laser cutting, and plasma bonding: all of them can be easily scaled up to an industrial size to enable the prototyping of the displays and improve the possibility of their usage in real applications. Hence, we demonstrated the possibility to integrate the presented process with standard industrial strategies, like the fabrication of flexible PCBs on which to incorporate the small resistors with direct writing of conductive materials. In addition, electronics for the activation of the display can be produced through standard PCB fabrication so that it can easily match with the connections of the flexible PCB underneath the display (connectors and electronic components easily available on the market).

The prototype was tested for up to one week of continuous taxel activation at 1 Hz with high-power pulses (25 ms - 1 Hz at 1 W nominal peak power, see Supplementary Fig. 6), demonstrating stable force values throughout the seven-day period. The primary failure mechanism observed was resistor breakage after prolonged and intense use. However, under normal operating conditions, no failures due to fatigue or wear-related issues were detected, including any delamination of the PDMS layer even after repeated use. Notably, the tests on human subjects were conducted with a limited number of samples, which were reused among participants, with each test session lasting approximately one to two hours, including possible device relocations.

The system has been demonstrated to be safe, operating under controlled conditions with fixed delivered power and precise timing. The energy delivered remains well below the heat perception threshold, as confirmed by the questionnaire results completed by all participants. Additionally, the system operates at temperatures significantly below the threshold for tissue damage. This can be verified by analyzing the maximum temperature reached during operation. When a single taxel is activated with a 0.5 s pulse at 10% PWM, the PDMS surface temperature in air (without skin contact) remains below 50 °C (see Supplementary Video, Fig. 2b, and the zoomed version in the Supplementary Fig. 3a, and Supplementary Fig. 11f). For reference, at 51 °C, the estimated exposure time threshold for tissue damage is 100 s, as reported in ref. 74. This threshold is 200 times longer than the duration of the activation pulse, ensuring thermal safety. Furthermore, due to the low thermal conductivity of PDMS, when in contact with the skin, the actual tissue temperature is expected to be substantially lower, further increasing the safety margin.

Noteworthy, the fabrication technique is very versatile, and it gives the possibility to explore in the future the development of larger displays composed of a higher number of dots to reproduce more complex sensations on the human skin, also related to the recognition of dynamic patterns. Even if the application shown in this work is focused on the representation of Braille characters on the users' fingertips, depending on the tactile perception threshold, it could be used to elicit tactile sensations to other body parts⁷⁵. For example, in virtual reality applications -ranging from healthcare to gaming and augmented reality -3,27,76 users often interact with digital objects by touching or grasping them. It is possible to create multiple displays, using one for each finger, and, thanks to their reduced thickness, easily integrate them into tight-fitting gloves, reproducing the tactile sensation generated by the virtual object and increasing the realism of these interactions. Moreover, the working principle and the proposed tactile display are fully modular, allowing the implementation of a larger number of active dots (larger matrix) with the aim of attaching larger displays on wider portions of the human body. The proposed device can thus also be used on the forearm or back of the hand, in order to provide more complex information through more sophisticated patterns. This versatility can facilitate integration with sensorized platforms for teleoperated tasks, where a robot is controlled remotely. For instance, delivering tactile feedback to the forearm could inform operators about proximity to obstacles or contact events during teleoperation⁷⁷. In biomedical applications, the use of tactile displays on the forearm of amputees with sensorized prostheses can provide closed-loop

sensory feedback, enhancing the quality and efficiency of grasping with a prosthetic hand 75,78 .

In conclusion, the results shown in this work confirm that this thermopneumatic activation system can be exploited for the development of fully portable and wearable refreshable tactile devices. Future perspectives include the possibility to investigate other parameters and features of the display. For example, other materials and even more scalable fabrication techniques can be considered, as well as more sophisticated dynamic models, even through the use of larger arrays, for more complex applications. This type of device also allows for in-depth studies on the sensations perceived by users, making it possible to provide more information, for example, on tactile perception thresholds and user reaction times to specific stimuli.

Methods

Materials

The commercial water-based Aerosol Conductive Ink NovaCentrix JS-A426 Silver Nanoparticle Ink (average size 30–40 nm) with a resistivity in the range 7.0 10^{-4} to 1.2 $10^{-5}~\Omega$ cm was purchased from NovaCentrix. Interconnection tracks between the printed layer and conductive copper wires were achieved by using a commercially available silver conductive paint (RS Components 186–3600, resistivity 0.001 Ω -cm). DuPont Kapton HN polyimide foils of 25 μ m thickness purchased from RS Components was employed as the printing substrate. PDMS films (10:1 ratio of base elastomer to curing agent, Sylgard 184 Dow Corning silicone elastomer base) was fabricated for later spin coating. A small thin stainless still lamina (80 μ m thickness, 6 ×8 mm² area) was attached on the backside of the transducer by using a small piece of Kapton tape, under the active dots, to increase local rigidity and thermal dissipation. Tegaderm medical tape (3 M Healthcare, Germany) was used to attach the display to the human skin.

Fabrication process

An Optomec Aerosol Jet print engine (Optomec Inc.) was engineered into a programmable 5-axis Cartesian stage controlled through a control code (G-Code) input to Aerotech A3200 Automation Controller, which moves the substrate below the aerosol. The linear translation stages (Thorlabs DDS300/M) provide a minimum incremental movement of 100 nm and a 300 mm travel distance in the XY plane. The manufacturing technique started with the direct aerosol jet printing of the conductive silver ink diluted with a 2:1 ratio of ink to DI water on the Kapton substrate attached to a glass slide, in order to fabricate the resistors⁷⁹. 1500 µL of the silver ink diluted with DI water with a 2:1 ratio were poured in the ultrasonic atomizer vial and a 200 µm nozzle was used. The printing parameters are: Sheath Flow Rate of 95 sccm, Atomizer Flow rate 18 sccm, Print Speed of the Conductive Paths 3 mm/s, Print Speed of the Resistors 0.3 mm/s. Once printed, the resistors are cured at 120 °C for 2 h for solvent evaporation and to enhance the conductivity - as reported in the datasheet of the Ag ink. The edges of the lateral paths and the central serpentines were then covered with some Kapton Tape in order to "protect" them from the following steps. A Kapton spacer, appositely cut with the laser cutter (speed 5%, Power 3%, Frequency 5000 for Epilog mini 24, 50 W CO2) was attached to the printed Kapton substrate by using double tape. In the following step, Nitrogen Plasma is carried out on the samples, in order to increase the adhesion between Kapton and later deposition of PDMS (Parameters for Nitrogen Plasma: minimum Power, 30 s exposure time)⁷⁰. PDMS is spin coated on the sample (time = 90 s acceleration = $85 \text{ m/s}^2 \text{ speed} = 1000 \text{ rpm}$) in order to obtain a thin deposited layer (nominal thickness 50 µm). The PDMS layer to use as the flexible membrane is obtained by spin coating (time = 90 s acceleration = $85 \text{ m/s}^2 \text{ speed} = 500 \text{ rpm}$) a glass slide covered with a sacrificial layer of poly(vinyl alcohol) (PVA) previously spin coated (time = 20 s acceleration = $85 \text{ m/s}^2 \text{ speed} = 1000 \text{ rpm}$) and cured at $80 \,^{\circ}\text{C}$ for 1 min (80 µm thick PDMS membrane). The layer of PVA is added in order to facilitate the peeling off of the PDMS layer from the glass slide. After this step, the pieces of Kapton tape are carefully removed and both the display sample and the PDMS membrane appositely cut to follow the display geometry underwent to Oxygen Plasma Treatment (50% of Maximum

Power and 30 s time, PE-25 Plasma System) in order to activate the layers of PDMS and create covalent bonds once put in contact^{80,81}. The bonding between PDMS layers ensures that inside the small cylinders of the Kapton spacer a closed volume of air is obtained. As a final step, silver conductive paint is manually applied to connect the conductive paths to copper wires, necessary for the activation of the device.

In the case of the flexible printed circuit, we designed the layout (reported in Fig. 3a) and the flex PCB was produced in outsourcing, using as starting material Pyralux AP9111 (by DuPont, US), an all-polyimide adhesiveless composite laminate of polyimide film bonded to copper foil. This specific material was selected because it exhibited the best adhesion with the silver nanoparticle ink used in this work. In contrast, printing tests conducted on other types of standard glued polyimide laminated for flexible PCB productionwere unsuccessful, as the printed resistors easily broken, likely due to the presence of a glue layer. AJP was used for fabricating the six heaters in order to complete the first layer of the device. After this step, we followed the same procedure described before, adding the laser-cut Kapton spacer with thin layer spin-coated PDMS - as described before – bonded to a 50 μ m commercial PDMS film from Wacker ELASTOSIL 2030 to obtain the final device (as reported in Fig. 3).

Morphological characterization

Thickness measurements were carried out with a DCM 3D Confocal Profilometer (Leica Microsystems), on purposely prepared samples. Optical images were taken by Olympus-BX53 microscope (Olympus), covering a magnification range from 2.5× to 50× and a Digital Microscopy Hirox KH-8700 digital microscope (Hirox, Japan).

Thermo-electro-mechanical characterization

Electrical. The resistance values, expressed in Ohm, were obtained by a two-point measurement across the device contacts with a Fluke "187 True RMS Multimeter" precision multimeter. The devices have been powered by using custom electronics during the characterization on the first prototype, so as to adjust power, PW, and F on purpose. The second prototype was characterized with the specifically designed portable electronic board with adjustable power.

Thermal. Thermal experiments were performed using a FLIR A300 thermal imaging camera (FLIR) and related ResearchIR 4 software (used for analysis and post-processing) acquired at 9 Hz. The samples were suspended in air during registration and activation. Pulsed power was applied to the device to record its response to different signals. In particular, the signals considered were: PW: 10 ms, F: 1 Hz, APW 10 mW; PW: 25 ms, F: 1 Hz, APW 25 mW; PW: 10 ms, F: 2 Hz, APW 50 mW; PW: 10 ms, F: 10 Hz, APW 100 mW, where APW is the average power of the actual applied signal.

Mechanical. Force measurements were performed using a customized system incorporating a load cell model LRF400 (0.25 lb full scale, by Futek, US), connected with a load cell amplifier (X200 gain, 10 V bridge excitation) and read out by with a NI-UBS 6009 DAQ card (National Instrument, US) and a custom developed software (developed with Visual Studio.NET, by Microsoft, US); the acquisition has been performed at 100 Hz, the root mean square noise of the measure was estimated to be in the order of $0.06\,\mathrm{mN}$. The fabricated device was attached to a glass slide and then placed horizontally under the load cell. The actuated part of the device was, by means of a manual micropositioner, placed in contact with the circular flat tip of the end effector (6.15 mm² area) mounted on the load cell (see Supplementary Fig. 16 in the Supplementary Information) in order to record the exerted force once reached a preload of 50 mN. As for thermal measurements, different pulsed powers were applied to the device to investigate the force response characteristics of the device. In particular, the activation signals considered were the same used during thermal tests: PW: 10 ms, F: 1 Hz, APW 10 mW; PW: 25 ms, F: 1 Hz, APW 25 mW; PW: 10 ms, F: 2 Hz, APW 20 mW; PW: 10 ms, F: 10 Hz, APW 100 mW, where APW is the average power of the actual applied signal, with also PW: 10 ms, F: 5 Hz, APW 50 mW and PW: 50 ms, F: 1 Hz, APW 50 mW in the case of the second prototype. Displacement measurements were performed using a ILD 1401-10 Laser Sensor (Micro-Epsilon Optronic GmbH, DE) interfaced through RS232 over USB connection with a custom developed software (developed with Visual Studio. NET, by Microsoft, US) acquiring at 1 kHz. The test has been performed on a device transferred on a glass slide, placed under the laser at working distance, focusing the spot directly onto the actuated region (a black permanent mark is applied on top of working area to have correct laser reflection for measurement). To characterize the expansion movements of the devices, the same pulsed power signals used for the force measurements were applied.

Portable electronics layout

To generate precisely adjustable constant power for the tactile display, a custom miniature electronic circuit (wearable power control board) has been designed and developed. This wireless power control board connects to a PC via Bluetooth using a suitable receiving dongle, enabling the creation of complex pulse patterns on demand through a custom software interface.

At the core of the device is the CYBLE-014008-00 Bluetooth Low Energy (BLE) module by Cypress/Infineon, which incorporates a PSoC4 microcontroller. This module generates driving pulses with configurable timing and patterns across six channels of the display. It also provides reference signal via an 8-bit Analog-to-Digital Converter (ADC), to enable precise power modulation. Communication with the PC is performed through a UART (Universal Asynchronous Receiver-Transmitter) over the BLE protocol.

Fixed pulsed power is generated by using a MAX4210 (by Maxim), a high-side power and current monitor that outputs a signal proportional to the power drown by the circuit. This output is fed into the negative input of an LM358 operational amplifier (by Texas Instruments), which operates in a feedback loop with a BCV27 Darlington transistor (by NXP). The transistor's emitter drives the common terminals of the six display taxel resistors, while their other terminals are connected to ground through a low- $R_{\rm on}$ N-channel MOSFET, a FQD13N10 (by Fairchild).

The microcontroller directly controls the MOSFET gates and sets the reference voltage at the positive input of the LM358 operational amplifier, allowing fine-tuned power delivery to the display taxels.

The complete schematics is reported in Supplementary Fig. 7, with also the layout of the implemented board.

Experimental protocol on subjects

For the experimental tests on the subjects, a specific Graphic User Interface (GUI), shown in Supplementary Fig. 14, was developed for the recording of the responses of the subject and for making the experiment more interactive. Once the device was attached to the subject's fingertip, all the dots were sequentially activated to preliminary check their working status and the level of perception of the subject. As mentioned in the main text, the Pulse Width and Period of the activation signal used during the experiments were 10 ms and 100 ms (10 Hz signal), with nominal peak power that varied during the tests in the range 120, 240, 360, 480, 600, 720, 840 mW. First, the subject was allowed to do 5 min of training with the maximum nominal peak power (840 mW), in order to relate the perceived sensation to the patterns. During the tests, the subject was asked to select on the GUI the pattern he perceived. The overall test is divided into three steps and all the patterns presented to all the subjects were randomly generated from the code.

The first part consists in presenting to the subject some patterns made by the activation of three specific dots: one pattern consists in the activation of the same dot for two times, with a pause of 600 ms in between the two – called "Same" in the subject interface; one with the activation of two close-by dots (#6 and #1 in Supplementary Fig. 13) – called "Near"; and one with the activation of two "far" dots (#6 and #4) – called "Far". This step was conducted with different levels of power, starting from the maximum (840 mW) to the minimum of 120 mW with a step of 120 mW. The 3

patterns - "same", "near", "far" - were presented in a random sequence of 5 patterns for each power level, with a total of 30 answers from the subject during this section of the test.

The second part of the test is more related to dynamic sensations: here clockwise, anticlockwise, up, and down patterns were presented to the subjects (patterns represented in Supplementary Fig. 13). The modality was the same described for the first step: a random sequence of 5 patterns among "clockwise", "anticlockwise", "up", "down" was generated and presented to the subject for all the 6 steps of the power – 120, 240, 360, 480, 600, 720, 840 mW – for a total of 30 answers from the subject.

The last part of the test is devoted to the identification of Braille characters. Specifically, we presented to the subject a random sequence of 30 characters generated from the collection of the six letters A, I, L, O, T, V (so as to present the same character 5 times). An example of activation of the letter T is shown in Fig. 5d and all the rest of the letter is reported in Supplementary Fig. 12. Here, two levels of power were investigated (840 mW and 480 mW), to check the difference in accuracy.

Lastly, the subjects were asked to fill in a questionnaire about the perceived sensation, the feeling of heat, and comfortability of the device.

Data availability

All data generated or analyzed during this study are included in this published article and its supplementary information files. Additional data related to this paper are available from the corresponding author upon reasonable request.

Received: 22 January 2025; Accepted: 17 May 2025; Published online: 16 July 2025

References

- Ko, S. H., Rogers, J., Ko, S. H. & Rogers, J. Functional materials and devices for XR (VR/AR/MR) applications. *Adv. Funct. Mater.* 31, 2106546 (2021).
- Sun, Z., Zhu, M., Lee, C. & Yang, Y. Progress in the triboelectric human–machine interfaces (HMIs)-moving from smart gloves to AI/ haptic enabled HMI in the 5G/IoT era. Nanoenergy Adv. 1, 81–120 (2021).
- Sun, Z., Zhu, M., Shan, X. & Lee, C. Augmented tactile-perception and haptic-feedback rings as human-machine interfaces aiming for immersive interactions. *Nat. Commun.* 13, 1–13 (2022).
- Pacchierotti, C. & Prattichizzo, D. Cutaneous/tactile haptic feedback in robotic teleoperation: motivation, survey, and perspectives. *IEEE Trans. Robot.* 40, 978–998 (2024).
- Yang, T. H. et al. Recent advances and opportunities of active materials for haptic technologies in virtual and augmented reality. Adv. Funct. Mater. 31, 2008831 (2021).
- Yu, X., et al. Skin-integrated wireless haptic interfaces for virtual and augmented reality. Nat 575, 473–479 (2019).
- Frediani, G. & Carpi, F. Tactile display of softness on fingertip. Sci. Rep. 10, 1–10 (2020).
- Lee, D. Y. et al. A wearable textile-embedded dielectric elastomer actuator haptic display. Soft Robot. 9, 1186–1197 (2022).
- Haynes, A., Simons, M. F., Helps, T., Nakamura, Y. & Rossiter, J. A wearable skin-stretching tactile interface for human-robot and human-human communication. *IEEE Robot. Autom. Lett.* 4, 1641–1646 (2019).
- Grasso, G. et al. Fully 3D-printed, stretchable, and conformable haptic interfaces. Adv. Funct. Mater. 33, 2213821 (2023).
- Frisoli, A. & Leonardis, D. Wearable haptics for virtual reality and beyond. *Nat. Rev. Electr. Eng.* 1, 666–679 (2024).
- Ishizuka, H., Hatada, R., Cortes, C. & Miki, N. Development of a fully flexible sheet-type tactile display based on electrovibration stimulus. *Micromachines* 9, 1–13 (2018).
- Blau, R. et al. Conductive block copolymer elastomers and psychophysical thresholding for accurate haptic effects. Sci. Robot. 9, 3925 (2024).

- Mazzotta, A., Carlotti, M. & Mattoli, V. Conformable on-skin devices for thermo-electro-tactile stimulation: materials, design, and fabrication. *Mater. Adv.* 2, 1787–1820 (2021).
- Li, K., Fang, Y., Zhou, Y. & Liu, H. Non-invasive stimulation-based tactile sensation for upper-extremity prosthesis: a review. *IEEE Sens.* J. 17, 2625–2635 (2017).
- Mizuhara, R., Takahashi, A. & Kajimoto, H. Combination of mechanical and electrical stimulation for an intense and realistic tactile sensation. In: Proceedings of the 17th ACM SIGGRAPH International Conference on Virtual-Reality Continuum and its Applications in Industry (ACM, 2019).
- Koo, I. M. et al. Development of soft-actuator-based wearable tactile display. *IEEE Trans. Robot.* 24, 549–558 (2008).
- Chen, Y. et al. Wearable actuators: an overview. Text 1, 283–321 (2021).
- Wu, X., Kim, S. H., Zhu, H., Ji, C. H. & Allen, M. G. A refreshable braille cell based on pneumatic microbubble actuators. *J. Microelectromechanical Syst.* 21, 908–916 (2012).
- Russomanno, A., Xu, Z., O'Modhrain, S. & Gillespie, B. A pneu shape display: Physical buttons with programmable touch response. In: *IEEE World Haptics Conference WHC*, 641–646 (IEEE, 2017).
- Akther, A. et al. Ultrasonic wave propagation of flexible piezoelectric polymer for tactile actuator: simulation and experiment. Smart Mater. Struct. 25, 115043 (2016).
- Guo, Y., Liu, L., Liu, Y. & Leng, J. Review of dielectric elastomer actuators and their applications in soft robots. *Adv. Intell. Syst.* 3, 2000282 (2021).
- Qu, X. et al. Refreshable Braille display system based on triboelectric nanogenerator and dielectric elastomer. Adv. Funct. Mater. 31, 2006612 (2021).
- Sîrbu, I.-D. et al. Electrostatic actuator for tactile display based on hydraulically coupled dielectric fluids and soft structures. SPIE 10966, 334–339 (2019).
- Stachiv, I., Alarcon, E. & Lamac, M. Shape memory alloys and polymers for MEMS/NEMS applications: review on recent findings and challenges in design, preparation, and characterization. *Met* 11, 415 (2021).
- Adilkhanov, A., Rubagotti, M. & Kappassov, Z. Haptic devices: wearability-based taxonomy and literature review. *IEEE Access* 10, 91923–91947 (2022).
- Yang, B. et al. A visual-tactile synchronized stimulation ring system for sensory rehabilitation integrating triboelectric sensing and pneumatic feedback. *Nano Energy* 135, 110638 (2025).
- Ankit et al. Soft actuator materials for electrically driven haptic interfaces. Adv. Intell. Syst. 4, 2100061 (2022).
- Chen, S., Chen, Y., Yang, J., Han, T. & Yao, S. Skin-integrated stretchable actuators toward skin-compatible haptic feedback and closed-loop human-machine interactions. *npj Flex. Electron.* 7, 1–12 (2023).
- 30. Li, D. et al. Touch IoT enabled by wireless self-sensing and haptic-reproducing electronic skin. Sci. Adv. 8, eade2450 (2022).
- 31. Li, D. et al. Miniaturization of mechanical actuators in skin-integrated electronics for haptic interfaces. *Microsyst. Nanoeng.* **7**, 1–9 (2021).
- Leroy, E. & Shea, H. Hydraulically Amplified Electrostatic Taxels (HAXELs) for Full Body Haptics. *Adv. Mater. Technol.* 2300242, https://doi.org/10.1002/ADMT.202300242 (2023).
- Chen, Y. et al. Wireless programmable patterns of electro-hydraulic haptic electronic skins able to create surface morphology. *Chem. Eng.* J. 500, 156612 (2024).
- Kajimoto, H. & Jones, L. A. Wearable tactile display based on thermal expansion of nichrome wire. *IEEE Trans. Haptics* 12, 257–268 (2019).
- 35. Yang, W. et al. A survey on tactile displays for visually impaired people. *IEEE Trans. Haptics* **14**, 712–721 (2021).

- Nadeem, M., Aziz, N., Sajjad, U., Aziz, F. & Shaikh, H. A comparative analysis of Braille generation technologies. In: *International Conference on Advanced Robotics and Mechatronics (ICARM)*, 294–299 (IEEE, 2016) https://doi.org/10.1109/ICARM.2016.7606935.
- Frey, B., Southern, C. & Romero, M. BrailleTouch: Mobile texting for the visually impaired. In: *Lecture Notes in Computer Science*, 6767 LNCS, 19–25 (LNCS, 2011).
- Aqel, M. O. A., Issa, A., Harb, A. & Shehada, J. Development of vibrotactile braille display and keyboard. In: *Proceedings of International Conference on Promising Electronic Technologies (ICPET)*, 28–33 (2019) https://doi.org/10.1109/ICPET.2019.00013.
- Russomanno, A., O'Modhrain, S., Gillespie, R. B. & Rodger, M. W. M. Refreshing refreshable braille displays. *IEEE Trans. Haptics* 8, 287–297 (2015).
- Liu, Z., Luo, Y., Cordero, J., Zhao, N. & Shen, Y. Finger-eye: a wearable text reading assistive system for the blind and visually impaired. In: *IEEE International Conference on Real-time Computing and Robotics* (RCAR), 123–128 (2016) https://doi.org/10.1109/RCAR.2016.7784012.
- Zhou, Z., Yang, Y. & Liu, H. A Braille Reading System Based on Electrotactile Display with Flexible Electrode Array. *IEEE CAA J. Autom. Sin.* 9, 735–737 (2022).
- 42. Tello, G., Choi, K., Kim, J. & Zhang, H. Design of a hands-free braille display using a pneumatically controlled wristband. In: *Proceedings of the IEEE Sensors* (IEEE, 2022).
- 43. Soule, C. W. & Lazarus, N. Reconfigurable Braille display with phase change locking. *Smart Mater. Struct.* **25**, 075040 (2016).
- Dong, X. et al. Multisensory flexible Braille interactive device based on liquid crystal elastomers. ACS Appl. Electron. Mater. 4, 3834–3840 (2022).
- Jang, S. Y. et al. Dynamically reconfigurable shape-morphing and tactile display via hydraulically coupled mergeable and splittable PVC gel actuator. Sci. Adv. 10, eadq2024 (2024).
- Mazzotta, A. & Mattoli, V. Ultrathin conformable electronic tattoo for tactile sensations. Adv. Electron. Mater. 9, 2201327 (2023).
- Wilkinson, N. J., Smith, M. A. A., Kay, R. W. & Harris, R. A. A review of aerosol jet printing—a non-traditional hybrid process for micromanufacturing. *Int. J. Adv. Manuf. Technol.* **105**, 4599–4619 (2019).
- Taccola, S. et al. Dual-material aerosol jet printing of magnetoresponsive polymers with in-process tailorable composition for smallscale soft robotics. *Adv. Mater. Technol.* 9, 2400463 (2024).
- Shin, J. et al. Thermo-pneumatic artificial muscle: air-based thermopneumatic artificial muscles for pumpless pneumatic actuation. *Soft Robot.* 11, 187–197 (2023).
- Werber, A. & Zappe, H. A thermo-pneumatically actuated tip-tiltpiston mirror. In: TRANSDUCERS 2007 - 2007 International Solid-State Sensors, Actuators and Microsystems Conference, 1525–1528 (IEEE, 2007) https://doi.org/10.1109/SENSOR.2007.4300435.
- 51. Lei, K. F., Chen, K. H. & Chang, Y. C. Protein binding reaction enhanced by bi-directional flow driven by on-chip thermopneumatic actuator. *Biomed. Microdevices* **16**, 325–332 (2014).
- Chee, P. S., Minjal, M. N., Leow, P. L. & Ali, M. S. M. Wireless powered thermo-pneumatic micropump using frequency-controlled heater. Sens. Actuators A Phys. 233, 1–8 (2015).
- Ahn, S. et al. Thermopneumatic Soft Micro Bellows Actuator for Standalone Operation. *Micromachines* 12, 46 (2021).
- Reimers, A. et al. Graphene-based thermopneumatic generator for on-board pressure supply of soft robots. Soft Robot. 12, 124–134 (2024).
- Zhang, B. & Sra, M. PneuMod: a modular haptic device with localized pressure and thermal feedback. *Proc. ACM Symp. Virtual Real. Softw. Technol. VRST* https://doi.org/10.1145/3489849.3489857 (2021).
- Qiu, Y., Lu, Z. & Pei, Q. Refreshable tactile display based on a bistable electroactive polymer and a stretchable serpentine joule heating electrode. ACS Appl. Mater. Interfaces 10, 24807–24815 (2018).

- 57. Puce, S. et al. A thermo-activated tactile micro-actuator for displays. *Microelectron. Eng.* **205**, 6–13 (2019).
- Kwon, H. J., Lee, S. W. & Lee, S. S. Braille dot display module with a PDMS membrane driven by a thermopneumatic actuator. *Sens. Actuators A Phys.* 154, 238–246 (2009).
- Fisher, C., Skolrood, L. N., Li, K., Joshi, P. C. & Aytug, T. Aerosol-jet printed sensors for environmental, safety, and health monitoring: a review. Adv. Mater. Technol. 8, 2300030 (2023).
- Li, G. et al. Precision Control of Aerosol Jet Printing for Conformal Electronics Fabrication with Ultra-Fine and Wide-Range Resolution. Adv. Mater. Technol. 2402114, https://doi.org/10.1002/ADMT. 202402114 (2025).
- Mazzotta, A., Taccola S., Harris R. A., Mattoli V. Finite element model of thermo-pneumatic transducers for wearable applications. In: 2024 IEEE International Flexible Electronics Technology Conference (IFETC), 1–3 (IEEE, 2024), https://doi.org/10.1109/IFETC61155.2024.10771872.
- Marburg Medium Braille Font Standard PharmaBraille. https://www. pharmabraille.com/pharmaceutical-braille/marburg-medium-fontstandard/ (2025).
- Hatzfeld, C. Haptics as an interaction modality. In: Hatzfeld, C., Kern,
 T. (eds) Engineering haptic devices. Springer series on touch and haptic systems, 29–100 (Springer, 2014).
- Lim, S. C., Kim, S. C., Kyung, K. U. & Kwon, D. S. Quantitative analysis of vibrotactile threshold and the effect of vibration frequency difference on tactile perception. In: SICE-ICASE International Joint Conference, 1927–1932 (IEEE, 2006) https://doi.org/10.1109/SICE.2006.315346.
- Islam, M. S. & Lim, S. Vibrotactile feedback in virtual motor learning: a systematic review. Appl. Ergon. 101, 103694 (2022).
- Hatzfeld, C. & Werthschützky, R. Vibrotactile force perception thresholds at the fingertip. In: Lecture Notes in Computer Science, 6191, 99–104 (LNCS, 2010).
- 67. WILSKA, A. On the vibrational sensitivity in different regions of the body surface. *Acta Physiol. Scand.* **31**, 285–289 (1954).
- Lindblom, U. Touch perception threshold in human terms of displacement amplitude on glabrous skin in stimulation with single mechanical pulses. *Brain Res.* 82, 205–210 (1974).
- Joshi, S., Loon, A., Van, Savov, A. & Dekker, R. Adhesion Improvement of Polyimide/PDMS Interface by Polyimide Surface Modification. MRS Adv. 1, 33–38 (2016).
- Francioso, L. et al. PDMS/kapton interface plasma treatment effects on the polymeric package for a wearable thermoelectric generator. ACS Appl. Mater. Interfaces 5, 6586–6590 (2013).
- Deshpande, A. et al. Integration of PDMS microfluidic channels with electronic systems using SIO2 mediated bonding of PDMS and polyimide. In: 25th International Conference on. Miniaturized Systems for Chemistry and Life Sciences, pp. 1231–1232 (µTAS, 2021).
- Hoang, M. V., Chung, H. J. & Elias, A. L. Irreversible bonding of polyimide and polydimethylsiloxane (PDMS) based on a thiol-epoxy click reaction. *J. Micromech. Microeng.* 26, 105019 (2016).
- Nolan, C. Y. & Kederis, C. J. Perceptual factors in Braille word recognition. Research Series No. 20, (American Foundation for the Blind. 1969).
- 74. Welch, A. J. The thermal response of laser irradiated tissue. *IEEE J. Quantum Electron.* **20**, 1471–1481 (1984).
- Jung, Y. H., et al. A wireless haptic interface for programmable patterns of touch across large areas of the skin. *Nat. Electron.* 5, 374–385 (2022).
- Zhu, M. et al. Haptic-feedback smart glove as a creative humanmachine interface (HMI) for virtual/augmented reality applications. Sci. Adv. 6, eaaz8693 (2020).

- Rodríguez-Sedano, F. J., Conde, M., Rodríguez-Lera, F. J. & Chaparro-Peláez, J. Measuring the impact of haptic feedback in collaborative robotic scenarios. *Univers. Access Inf. Soc.* 23, 1031–1049 (2024).
- Sariyildiz, E. et al. Experimental evaluation of a hybrid sensory feedback system for haptic and kinaesthetic perception in hand prostheses. Sensors 23, 8492 (2023).
- 79. Ratnayake, D., Curry, A. & Walsh, K. Demonstrating a new ink material for aerosol printing conductive traces and custom strain gauges on flexible surfaces. In: *IEEE International Conference on Flexible and Printable Sensors and Systems (FLEPS)* (2021).
- Lunni, D., Cianchetti, M., Filippeschi, C., Sinibaldi, E. & Mazzolai, B. Plant-inspired soft bistable structures based on hygroscopic electrospun nanofibers. Adv. Mater. Interfaces 7, 1901310 (2020).
- 81. Borók, A., Laboda, K. & Bonyár, A. PDMS bonding technologies for microfluidic applications: a review. *Biosens* **11**, 292 (2021).

Acknowledgements

Not applicable.

Author contributions

A.M., I.C, and V.M. conceived the research. A.M., S.T., and M.S.S. contributed to the fabrication of the devices and their optimization. A.M. conducted the characterization, data analysis, and experiments on subjects. A.M. and V.M. developed the electronics and software. R.A.H. and V.M. supervised the work. A.M. wrote the first draft and all authors discussed and revised the manuscript.

Competing interests

The authors declare no competing interests.

Additional information

Supplementary information The online version contains supplementary material available at https://doi.org/10.1038/s41528-025-00426-3.

Correspondence and requests for materials should be addressed to A. Mazzotta, S. Taccola or V. Mattoli.

Reprints and permissions information is available at http://www.nature.com/reprints

Publisher's note Springer Nature remains neutral with regard to jurisdictional claims in published maps and institutional affiliations.

Open Access This article is licensed under a Creative Commons Attribution 4.0 International License, which permits use, sharing, adaptation, distribution and reproduction in any medium or format, as long as you give appropriate credit to the original author(s) and the source, provide a link to the Creative Commons licence, and indicate if changes were made. The images or other third party material in this article are included in the article's Creative Commons licence, unless indicated otherwise in a credit line to the material. If material is not included in the article's Creative Commons licence and your intended use is not permitted by statutory regulation or exceeds the permitted use, you will need to obtain permission directly from the copyright holder. To view a copy of this licence, visit http://creativecommons.org/licenses/by/4.0/.

© Fondazione Istituto Italiano di Tecnologia, and Silvia Taccola, Midori Sanchez Sifuentes, Russell A. Harris 2025